DEVELOPMENT OF A DESIGN TOOL FOR SMALL OFF-ROAD UNMANNED WHEELED GROUND VEHICLES: A CASE STUDY

William Smith,[*] Huei Peng,[†] Zoran Filipi,[‡] Denise Kramer,[§] and Mike Pozolo[**]

Small unmanned ground vehicles (SUGVs) are used more than ever before in fields ranging from planetary exploration to combat. The success of these vehicles depends largely on their energy system performance. In order to maximize the effectiveness of SUGVs and their mission success rate, energy system performance must be considered in the original design of the vehicle. For this reason an early-stage design tool for off-road skid-steering wheeled SUGVs was developed. The tool provides the user immediate feedback regarding the effect of vehicle and mission parameters on the system's feasibility and efficiency. The design tool uses the fundamentals of energy conservation, component scaling laws, and the theory of terramechanics to determine system feasibility over a variety of operating conditions. This step can eliminate designs which would fail due to insufficient tractive force or energy supply, for example. Further analysis examines the tradeoff between any two vehicle parameters on system performance. In particular, this step is useful for analyzing the interdependence of motor size and transmission ratio on system feasibility and efficiency. Finally, the tool can quickly optimize both design and control for a predetermined mission (distance, elevation profile, soil type). Given a range of vehicle parameter values, all design combinations are compared to find the optimal solution using a predefined velocity profile. Then, using the optimal vehicle design, the velocity profile is treated as a control parameter and optimized for the mission while maintaining total travel time. This process iterates until the solution converges. The design tool can help eliminate poor vehicle designs early in the process, lead to more robust designs capable of performing in a variety of operating conditions, and provide insight into the benefits of autonomous operation through flexibility in vehicle speed.

INTRODUCTION

Small unmanned ground vehicles (SUGVs) are being incorporated into many fields, including space exploration, search and rescue, and combat. SUGVs are asked to perform in off-road, rugged, dangerous environments where mission success is critical. Common failure modes include the vehicle becoming trapped due to soft-soil wheel sinkage and insufficient energy supply, especially when the vehicle's energy supply is limited.[1] In order to meet mission range, duration, and

[*] PhD Candidate, Department of Mechanical Engineering, The University of Michigan, Ann Arbor, MI.
[†] Professor, Department of Mechanical Engineering, The University of Michigan, Ann Arbor, MI.
[‡] Research Professor, Department of Mechanical Engineering, The University of Michigan, Ann Arbor, MI.
[§] Powertrain Modeling & Simulation, CASSI Analytics, U.S. Army RDECOM-TARDEC, Warren, MI.
[**] Team Leader, Powertrain Modeling & Simulation, CASSI Analytics, U.S. Army RDECOM-TARDEC, Warren, MI.

task requirements the vehicle must be systematically designed. It is necessary to be able to predict the vehicle's performance in these situations, given the importance of these missions. Given the multitude of design choices and potential operating conditions, and the complexities inherent with off-road driving, it can be difficult to select the right vehicle parameters early in the design process. This is why the Off-Road Robot Design Tool (ORRDT) was developed for small skid-steering wheeled vehicles. ORRDT uses the principles of energy conservation, component scaling laws, and the theory of terramechanics to determine system feasibility and efficiency. The goal of ORRDT is to increase mobile robot mission life through consideration of power and energy in vehicle design and control.

An important component of ORRDT is load characterization. For many vehicles, propulsion is the dominant load. This is especially true for off-road vehicles, where resistance forces are significantly higher than for road vehicles. Unlike road vehicles, where the relationship between the pneumatic tires and hard road surface can be characterized using a constant coefficient of friction for many conditions, off-road wheel-terrain interaction is much more complex. The study of off-road vehicle-terrain interaction, termed "terramechanics", began in the mid-20th-century by Bekker.[2,3] These principles have since been expanded upon by others,[4,5] particularly Wong, whose equations are used primarily in this paper. The use of terramechanics allows for determining thrust and resistance forces for each wheel given the current operating condition.

The theory of terramechanics has been used in the research of off-road ground vehicles, often with favorable comparisons to experimental data.[6,7] While it has been shown that current terramechanics theory can be significantly less accurate for very small vehicles, no better alternative exists.[8] As small unmanned vehicles increase in importance, more fundamental research for small wheel-soil interaction is necessary. Before a vehicle is built and experimentally tested, it should be simulated in a representative environment. Bauer developed a planetary rover chassis simulation tool, coupling rigid multi-body dynamics with wheel-soil terramechanics modeling.[9] Through parameter tuning, the sinkage-wheel slip relationship was accurately modeled, while motor torque and drawbar pull showed significant correlation. Several other researchers have created similar simulation tools.[10, 11] The usefulness of each simulation tool could be improved by adding additional analysis before the vehicle model is first developed.

Before a complex simulation tool is used, use of a design tool focused on system feasibility and efficiency could lead to better initial designs, saving the user time. Previous design tools which been developed include *RMPET*, a rover chassis evaluation tool using Bekker terramechanics theory to predict performance for wheeled, tracked, and legged locomotion systems over a variety of soils and surfaces.[12] In another example, a mobility analysis tool was developed, again using Bekker terramechanics theory, to evaluate mobility of a vehicle operating off-road.[13] Both of these design tools give the user a great resource in the early stages of design, before more complex simulation or testing. The design tool discussed in this paper, ORRDT, varies from previous design tools through its calculation of terramechanics equations, method of data presentation, and use of combined optimization on design and control. The terramechanics equations are calculated offline and stored in a series of lookup tables for each wheel. ORRDT consists of three stages, all of which use the lookup tables to rapidly calculate system performance. The details of wheel table generation and each stage of the design tool are discussed later in the paper.

THEORY OVERVIEW

Design of a vehicle requires making many design choices, the combination of which determines not only the performance of the vehicle, but even the operation feasibility for certain soil types. Vehicle design requires more than intuition, due to the complex nature of wheel-soil inter-

actions and the number of design parameter combinations. ORRDT was designed to simultaneously evaluate the performance and feasibility of many design parameter combinations, and provide the information in a way the user can easily understand. To focus on the effects of each design parameter, some simplifications were taken.

Vehicle Model

A simple vehicle model, shown in Figure 1, was chosen to simplify calculations, increase processing speed, and prevent unnecessary model complexity. The vehicle model does not include suspension parameters or pitch moments, the terrain is flat and even (vehicle can pitch but not roll), and motion is limited to the longitudinal direction.

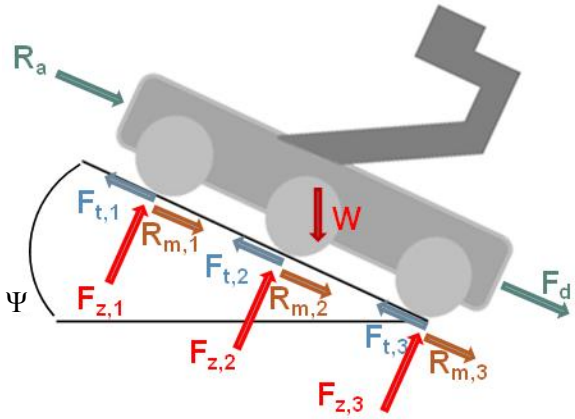

Figure 1. Vehicle Model (shown with 3 axles).

Vehicle dynamics can largely be summarized by Eq. (1), which uses Newton's second law. Forces $F_{z,w}$ are the normal loads for each wheel. When the vehicle contains more than two axles it is assumed that the normal load varies linearly from front to rear. ORRDT does not consider situations which would result in loss of ground contact for any wheel, as this would significantly alter the vehicle dynamics.

$$mass \cdot acceleration = \sum_{w=1}^{No.\ Wheels}\left[F_{t,w} - R_{m,w}\right] - R_{air} - F_{drawbar} - R_{gravity} \tag{1}$$

$$F_{t,w} = wheel\ thrust\ force \tag{2}$$

$$R_{m,w} = wheel\ motion\ resistance\ force \tag{3}$$

$$R_{air} = aerodynamic\ resistance = \frac{\rho}{2} \cdot C_D \cdot A_f \cdot Velocity^2 \tag{4}$$

$$F_{drawbar} = drawbar\ pull = \sum_{w=1}^{No.\ Wheels}\left[F_{thrust}\right] - \Sigma R \tag{5}$$

$$R_{gravity} = gravitational\ resistance = mass \cdot gravity \cdot \sin\Psi \tag{6}$$

Terramechanics Modeling

For a given operating condition, all terms in Eq. (1) are known except for the wheel forces. Wheel thrust and resistance forces are found by integrating the shear (τ) and normal (σ) stress along the interface between the wheel and soft soil, as illustrated in Figure 2.[14] The equations assume the wheel is harder than the soil, so that deformation occurs primarily in the soil. The soil parameter values used for this case study can be found in the Appendix.

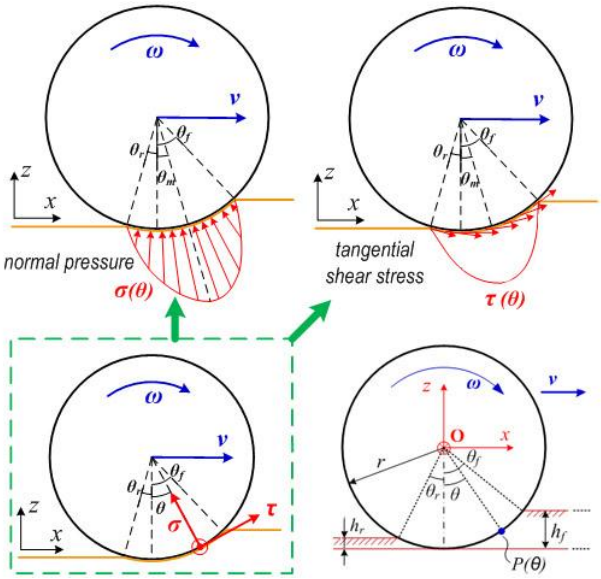

Figure 2. Description of Stresses Acting on Wheels.[15]

Equations (7) and (8) describe the calculation of the thrust and resistance forces occurring at the wheel-soil interface. Equation (9) describes the calculation of the normal force at each wheel. θ_f is the entry contact angle, where the ground and wheel surfaces first intersect. θ_r is the rear contact angle, where the ground and wheel surface last intersect. It was assumed the soil did not elastically rebound after loading, resulting in a θ_r value of 0. Thrust and resistance forces are assumed to act parallel with the ground, while the normal load acts perpendicular to the ground.

$$F_{thrust} = b \cdot r \int_{\theta_r}^{\theta_f} \tau(\theta, s) \cdot \cos\theta \, d\theta \tag{7}$$

$$F_{resist} = b \cdot r \int_{\theta_r}^{\theta_f} \sigma(\theta, s) \cdot \sin\theta \, d\theta \tag{8}$$

$$F_{normal} = b \cdot r \int_{\theta_r}^{\theta_f} (\sigma(\theta, s) \cdot \cos\theta + \tau(\theta, s) \cdot \sin\theta) d\theta \tag{9}$$

Normal Stress

The normal stress at each point along the wheel-soil interface, characterized by Eq. (10), is dependent on the amount of wheel sinkage *z*.

$$\sigma(\theta, s) = \left(\frac{k_c}{b} + k_\phi\right) z(\theta, s)^n \tag{10}$$

Normal stress increases in magnitude from zero at the entry angle θ_f to its maximum at θ_m (assumed to be the location of both maximum shear and normal stress). Normal stress increases over this region, termed the front-region, in a bow-like shape. Over the rear-region, from θ_m to θ_r, normal stress has the same characteristics.[16] Thus a front-region equivalent angle, θ_{eq} is used to calculate *z* over the rear contact region. When the wheel is used to brake the vehicle, the slip val-

ue s will become negative. When this occurs the soil dynamics fundamentally alter, which requires alteration of Eq. (13).[14]

$$z(\theta,s)=\begin{cases} r\left(\cos\theta-\cos\theta_f\right), & \theta_m(s)\le\theta\le\theta_f \\ r\left(\cos\theta_{eq}-\cos\theta_f\right), & \theta_r(s)\le\theta<\theta_m(s)\end{cases} \tag{11}$$

$$\theta_{eq}(\theta)=\theta_f-\frac{\theta-\theta_r}{\theta_m-\theta_r}\cdot\left(\theta_f-\theta_m\right) \tag{12}$$

$$\theta_m(s)=\begin{cases}(a_0+a_1\cdot s)\theta_f, & s>0\\ \cos^{-1}\left(\dfrac{1+s}{\sqrt{1+\tan^2\left(\frac{\pi}{4}-\frac{\phi}{2}\right)}}\right)+\tan2^{-1}\left(-\tan\left(\frac{\pi}{4}-\frac{\phi}{2}\right),1\right), & s<0\end{cases} \tag{13}$$

$$\theta_r(s)=(b_0+b_1\cdot s)\theta_f \tag{14}$$

$$s=\begin{cases}{(\omega\cdot r-v)}/{(\omega\cdot r)}, & |\omega\cdot r|>|v|\\ {(\omega\cdot r-v)}/{v}, & |\omega\cdot r|<|v|\end{cases} \tag{15}$$

Equation (10) makes the assumption that the soil is undisturbed when first contacted. It is necessary to alter the equation for wheels in a tandem configuration in that the terrain does not recover completely after impacted by the first wheel. This affects the initial pressure-sinkage relationship for the second wheel, as shown in Figure 3. The soil begins unloading at point A, followed by reloading at point B. This process is repeated with points C and D. The normal load during unloading and reloading is expressed in Eq. (16), where z_u is the sinkage at unloading.

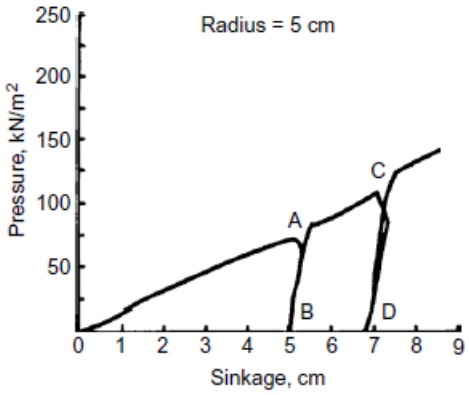

Figure 3. Response to Repetitive Normal Load of a Mineral Terrain.[14]

$$\sigma_{(un)loading}(\theta,s)=\left(\frac{k_c}{b}+k_\phi\right){z_u}^n-(k_o+A_u\cdot z_u)(z_u-z(\theta,s)) \tag{16}$$

Shear Stress

The shear stress can be characterized by the following Eq. (17), dependent upon the soil type properties.

$$\tau(\theta) = \begin{cases} sgn(j) \cdot \tau_{max} \cdot \left[1 - e^{-\left(|j|/K\right)}\right], & soil\ A \\ sgn(j) \cdot \tau_{max} \cdot \left(|j|/K_w\right)\left[1 - e^{-\left(|j|/K_w\right)}\right], & soil\ B \\ sgn(j) \cdot \tau_{max} \cdot (K_r)\left[1 + \left[\frac{1}{K_r(1 - 1/e)} - 1\right] \cdot e^{-\left(|j|/K_w\right)}\right]\left[1 - e^{-\left(|j|/K_w\right)}\right], & soil\ C \end{cases} \quad (17)$$

Soil Type A) The shear curve does not display a 'hump' of maximum shear stress, but rather the shear stress increases with shear displacement and approaches a constant value.

Soil Type B) The shear curve exhibits a 'hump' of maximum shear stress and then the shear stress decreases continually with the increase of shear displacement, such as observed in the shearing of muskeg mat.

Soil Type C) The shear curve displays a 'hump' of maximum shear stress and then decreases with the increase of shear displacement to a constant value of residual stress.

For all terrain types the maximum shear stress is characterized by Eq. (18).

$$\tau_{max} = c + \sigma(\theta) \cdot \tan\phi \quad (18)$$

Eq. (17) requires knowledge of the shear displacement, j along the wheel circumference. This value can be calculated by integrating the shear rate given by Eq. (19).

$$v_j(\theta) = r\omega - v\cos\theta = \begin{cases} r\omega[1 - (1 - s)\cos\theta\,], & |\omega \cdot r| > |v| \\ r\omega\left[1 - \frac{1}{1 + s}\cos\theta\,\right], & |\omega \cdot r| < |v| \end{cases} \quad (19)$$

$$j(\theta) = \int_0^t v_j(\theta)dt = \int_\theta^{\theta_f} v_j(\theta)\frac{1}{\omega}d\theta \quad (20)$$

$$= \begin{cases} r\left[\left(\theta_f - \theta\right) - (1 - s)\left(\sin\theta_f - \sin\theta\right)\right], & |\omega \cdot r| > |v| \\ r\left[\left(\theta_f - \theta\right) - \frac{1}{(1 + s)}\left(\sin\theta_f - \sin\theta\right)\right], & |\omega \cdot r| < |v| \end{cases}$$

Wheel Tables

The previously described terramechanics equations are nonlinear and not closed-form. Calculation of force outputs requires integration of the stresses from the entry angle to the exit angle. A forward looking set of equations, where normal load and driving torque are inputs rather than outputs, is not directly obtainable. Common methods for handling this situation are to iterate wheel sinkage until the desired normal load is obtained or to linearize the normal and shear stress equations (producing a closed-form solution).[17,18] These methods are undesirable due to computation time and loss of fidelity, respectively.

Instead of using either of these methods, lookup-tables of the terramechanics equations were created for all desired wheel-terrain combinations. The methods for building and using these tables are described in Figures 4 and 5. Instead of integrating the normal and shear stresses, followed by iterating to find the correct normal load (at each step), the computation time is largely up front in the creation of the tables. At each step there are three 3-dimensional interpolations, one 2-dimensional interpolation, and three 1-dimensional interpolations required. The improvement in computational efficiency allows for ORRDT to perform vector computations very quickly. Example wheel tables (radius = 0.1m, width = 0.1m, soil type = loose air dried sand) can be found in the Appendix. Vector computations can be performed over a range of vehicle designs and operating conditions, or over an entire drive cycle.

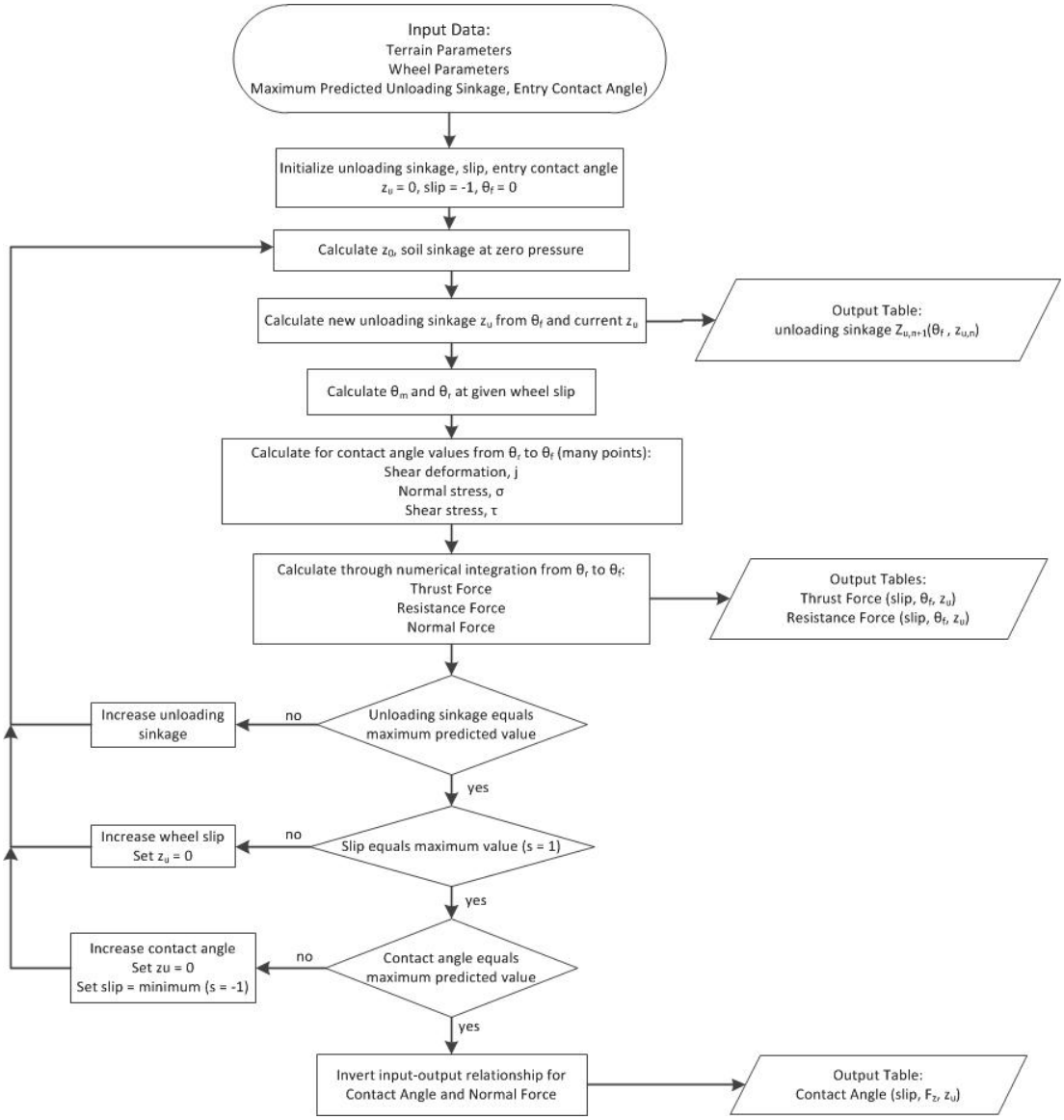

Figure 4. Flow Chart for Building Wheel Tables.

CASE STUDY

This case study serves the purpose of showing how ORRDT can be useful to a small vehicle designer. A list of desired specifications and operating conditions are given in Tables 1 and 2.

Table 1. Case Study Vehicle Specifications and Operating Conditions

vehicle length (m)	vehicle width (m)	cg height (m)	drag coefficient (est)
1.5	0.5	0.25	0.5

soil types	payload capacity (kg)	cruising range (km)
loose air-dried sand, medium soil, clayed soil	5	25

Table 2. Case Study Operating Conditions

operating condition	slope (radians)	velocity (m/s)	acceleration (m/s^2)
1: slope traversal	0.08	0.1	0
2: cruising range	0	5	0

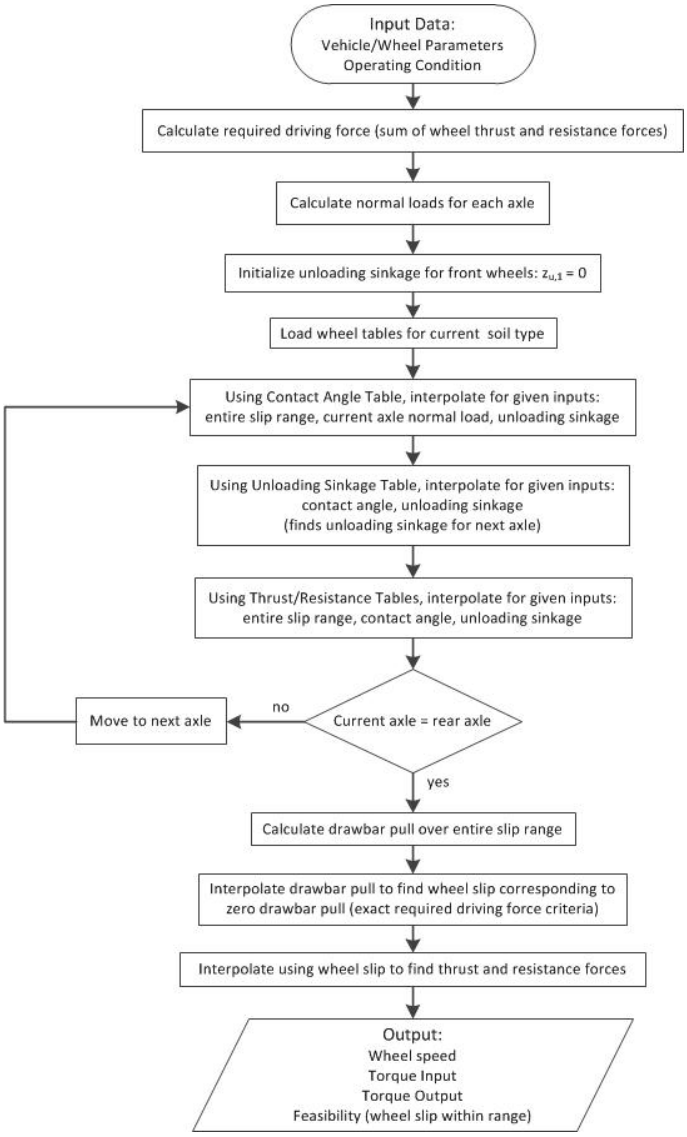

Figure 5. Flow Chart for Using Wheel Tables.

DESIGN TOOL

The Off-Road Robot Design Tool (ORRDT) uses the Wheel Lookup Tables, described in the previous section, to give rapid feedback regarding system feasibility and efficiency resulting from vehicle design choices. ORRDT consists of three stages, each with a unique purpose. Stage 1 examines system feasibility based on total system mass, a key vehicle property in terramechanics equations. Stage 2 allows the user to select a performance measure, such as energy required, as a

function of two vehicle parameters. Stage 3 compares vehicle performance of a range of vehicle configurations for a predetermined mission profile. This stage allows for vehicle design optimization, as well as velocity profile optimization for particular vehicle configuration.

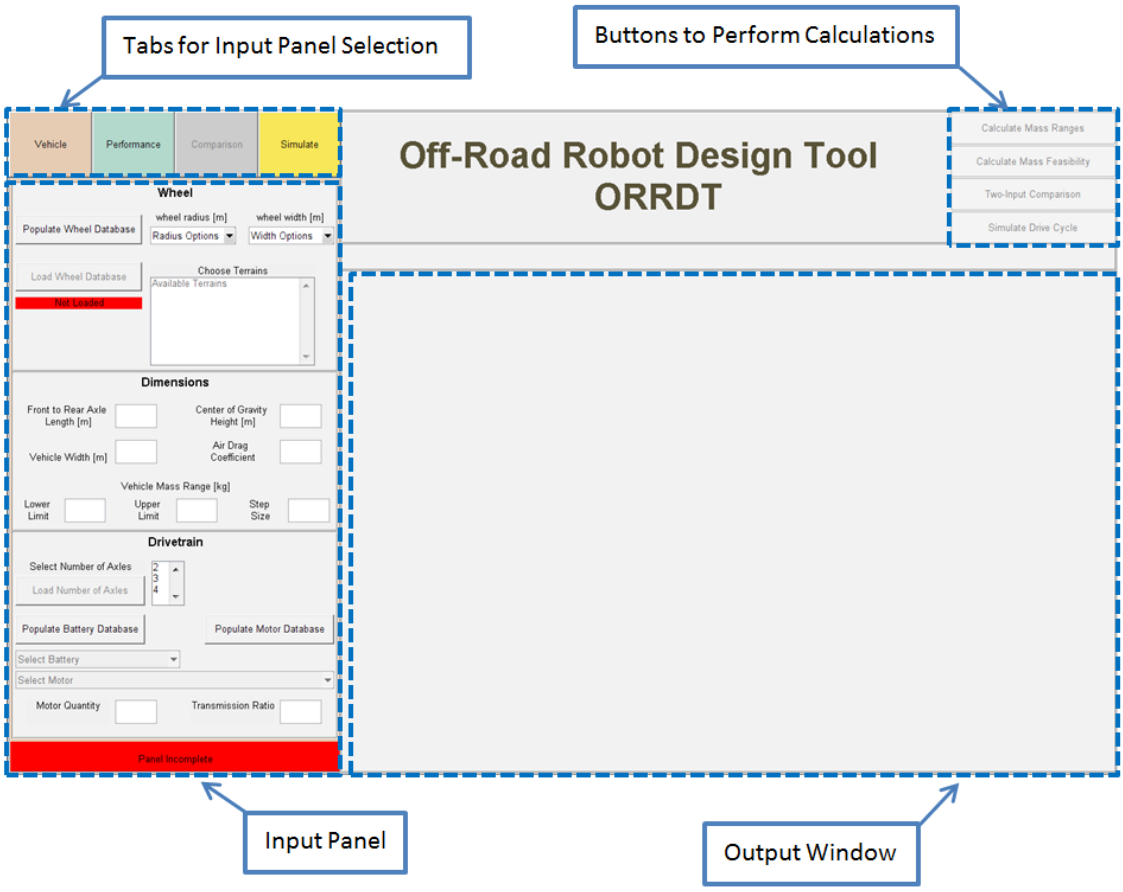

Figure 6. ORRDT Main Window.

Stage 1: Mass Feasibility

In the first stage of the design process, the users inputs the vehicle specifications and operating conditions into the "Vehicle" and "Performance" panels. The case study parameters were entered into these panels, as shown in Figure 7. Within the first stage there are two buttons available to produce an output, located in the top right of the main window. The first button, labeled "Calculate Mass Ranges," determines the total vehicle mass feasibility region for each terrain, operating condition, and number of axles. The algorithm uses electric motor scaling laws from University of Michigan Professor Heath Hofmann (personal communication, February 17, 2011),* along with battery-type specific power and energy values.† This process is outlined in Figure 8.

* The specifics of the electric motor scaling laws will appear in a future publication, and cannot be listed here.
† Lithium-Ion battery assumed to have specific power and energy equal to 300 W/kg and 100 W-hr/kg, respectively.[19]

Figure 7. Vehicle (left) and Performance (right) Panels.

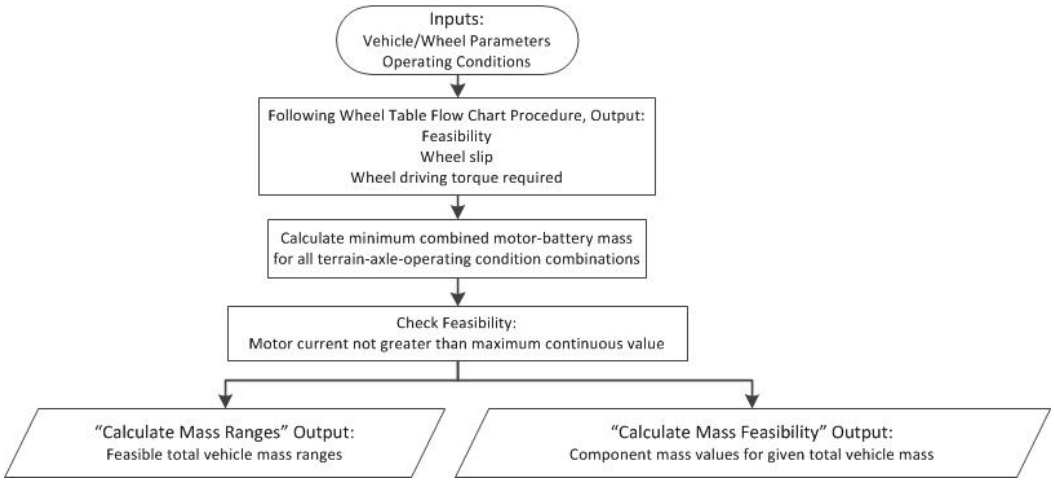

Figure 8. Flow Chart of Stage 1 Algorithm.

Figure 9 shows that under the vehicle mass range of interest, the slope traversal operating condition is the most restrictive. Clayed soil is the most demanding of the three soil types chosen, while the entire vehicle mass range is feasible over dry sand.

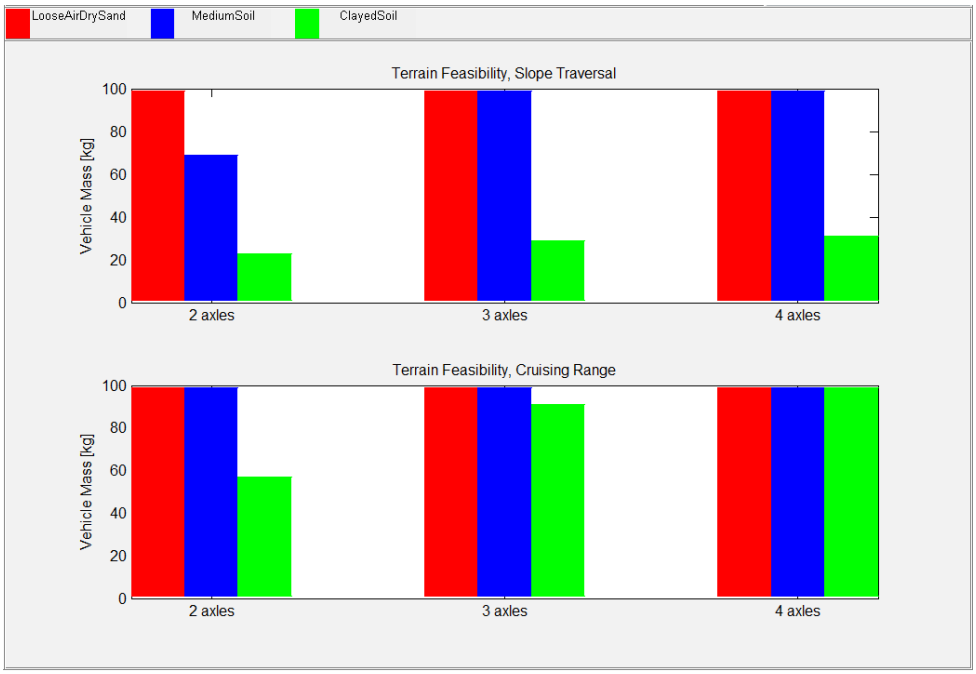

Figure 9. "Calculate Mass Ranges" Output.

The second button available in Stage 1, labeled "Calculate Mass Feasibility," is used to determine if the previously determined feasible vehicle mass values, shown in Figure 9, are feasible based on the component mass values. For each number of axles the wheel mass is added to the motor and battery mass values, the sum of which is minimized for the most challenging soil type and operating condition. If the component mass sum is less than the total vehicle mass, the remainder is shaded in magenta. If, however, the sum is greater than the total vehicle mass, the overrun is shaded in cyan. The user must determine if the amount of "remaining" mass available is enough for the vehicle chassis, controllers, and any additional components.

Using both buttons in Stage 1, along with the wide selection of vehicle parameters and operating conditions, the user should be able to select vehicle parameters which robustly meet the performance specifications. For instance, the user may increase the wheel radius if the vehicle chassis mass will exceed the total mass limit. If an acceptable vehicle design cannot be found, the difficulty of the operating conditions may need to be adjusted; perhaps through a decrease in the terrain slope.

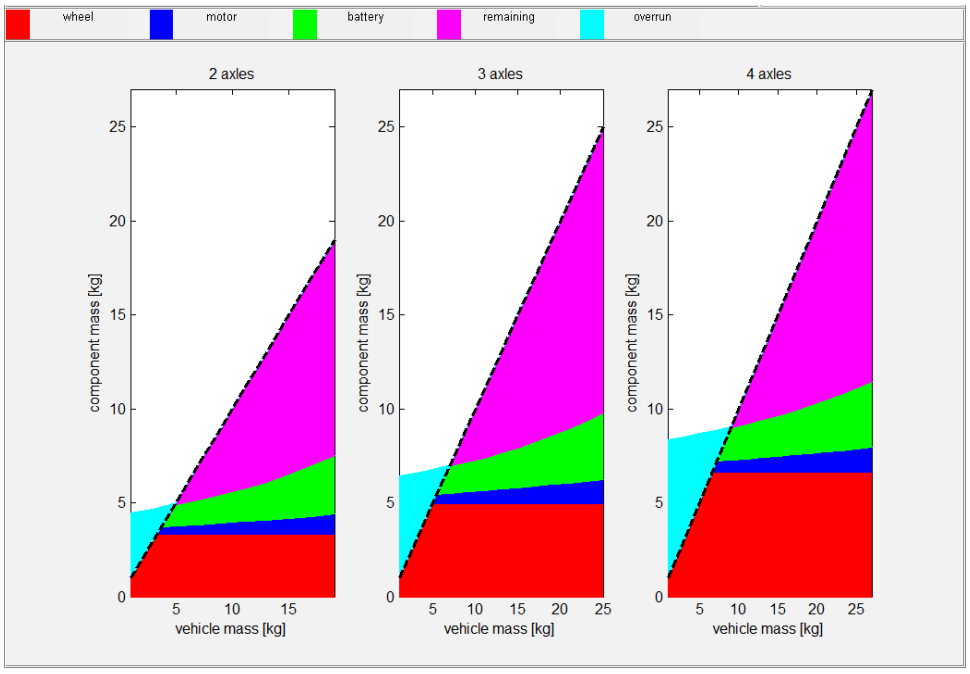

Figure 9. "Calculate Mass Feasibility" Output.

Stage 2: Two-Parameter Comparison

Once the user feels comfortable with the vehicle design, further tuning is possible during Stage 2. Here the user can select any two input parameters, from motor scaling factor to operating speed, and compare any output performance, from energy requirement to wheel slip. This step should not only help with the user's design intuition, but help examine the tradeoffs inherent in many critical design decisions. When the comparison is made, all other parameters must be individually selected. While the first stage largely helps select wheel parameters to meet terramechanics feasibility, the second stage can help choose the motor scaling factor and transmission ratio. It is important to size the motor while considering the transmission ratio, as the expected operating conditions will significantly change the motor efficiency. Figure 10 shows energy requirement (kW-s/km) as a function of motor scaling factor and transmission ratio for the two operating conditions. The color range of the output plot can be adjusted manually, which can be necessary since the energy requirement can become orders of magnitude larger than the minimum value.

Examining the energy requirement for the two operating conditions shows the "slope traversal" condition requires more energy and a larger electric motor at maximum efficiency. Selecting a motor scaling factor and transmission ratio based on the "cruising range" condition might result in near-infeasibility when operating on a slope. The output plots allow the user to determine the correct combination of motor size and transmission ratio based on the expected vehicle operation and necessary robustness against failure.

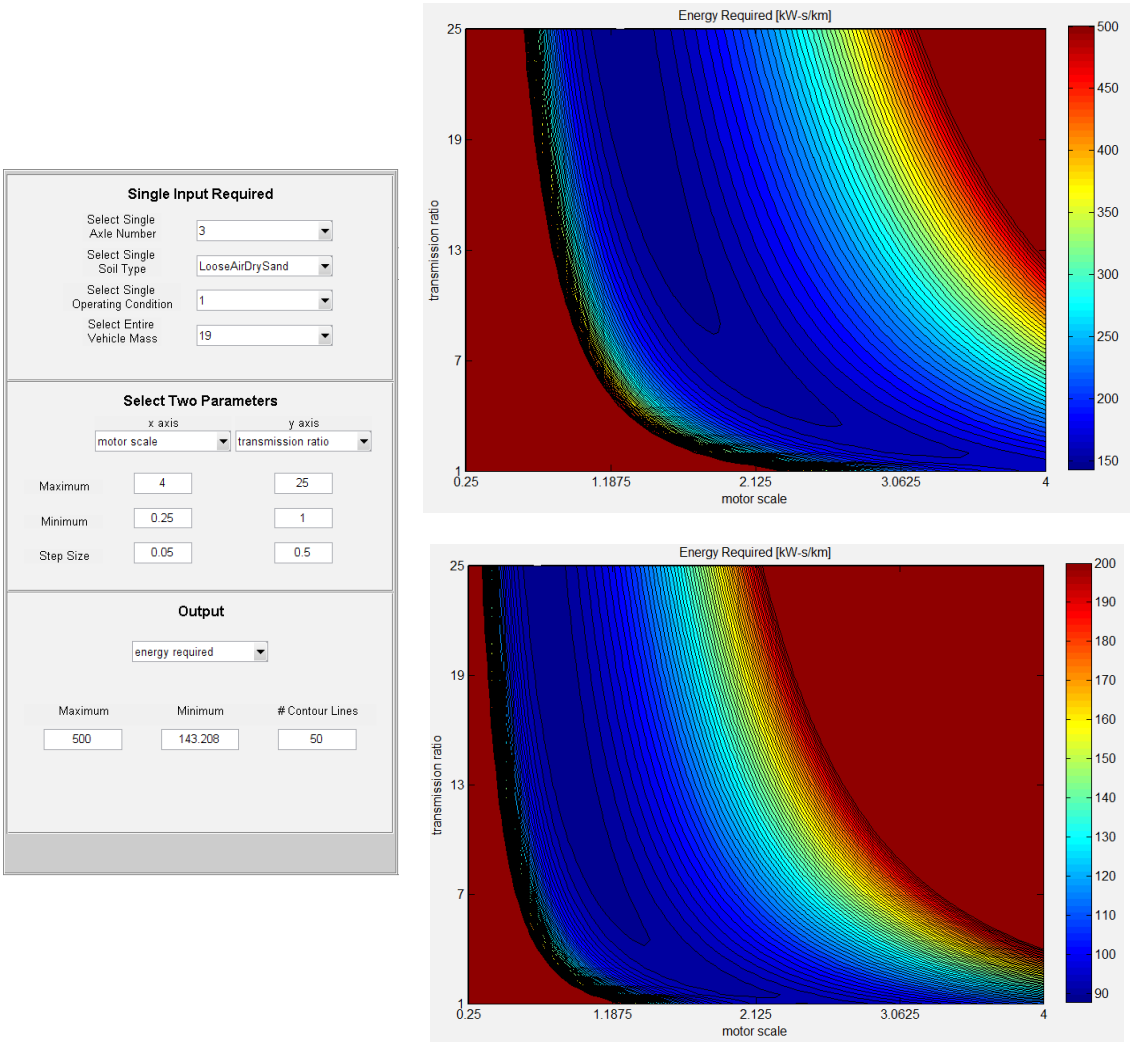

Figure 10. Comparison Panel (left) and "Two-Input Comparison" Output for Operating Conditions 1 and 2 (right, top and bottom, respectively).

Stage 3: Design & Control Optimization

While examining individual operating conditions is very useful, exploring performance over an extended drive cycle can provide additional information. By selecting a representative drive cycle, consisting of the terrain elevation profile, soil types, and velocity, mission performance of several vehicle designs can be compared. The use of drive cycles to compare performance is commonly used for passenger vehicles by the Environmental Protection Agency, displayed as "miles-per-gallon" for a representative city and highway cycle. The user first selects the drive cycle terrain profile and initial velocity profile. Then, using expected feasible vehicle parameter ranges, the "Simulate Drive Cycle" button calculates the performance of each vehicle design combination. Key performance metrics, such as maximum wheel slip and total energy consumption, are displayed in the output window. A "Cost" is calculated using a linear combination of energy efficiency (kW-s/km) and maximum wheel slip. The cost value balances vehicle efficiency and robustness, since the vehicle's mobility limits correspond to wheel slip.

The vehicle design which has the lowest cost appears above the list of all vehicle design combinations. Using the "optimal" design, the velocity profile can be optimized by selecting "Optimize Velocity." ORRDT then uses the constrained nonlinear optimization function *fmincon* in MATLAB to find the velocity profile which minimizes the total cost of for the optimal vehicle design operating on the terrain profile. The velocity profile is constrained so that total travel time is held constant.

The process can be iterated by selecting "Iterate Design," which calculates the performance of all vehicle designs using the optimal velocity profile. Iterating also allows the user to narrow the parameter range to better find the optimal design solution. Figure 11 shows the ORRDT main window after three iterations.

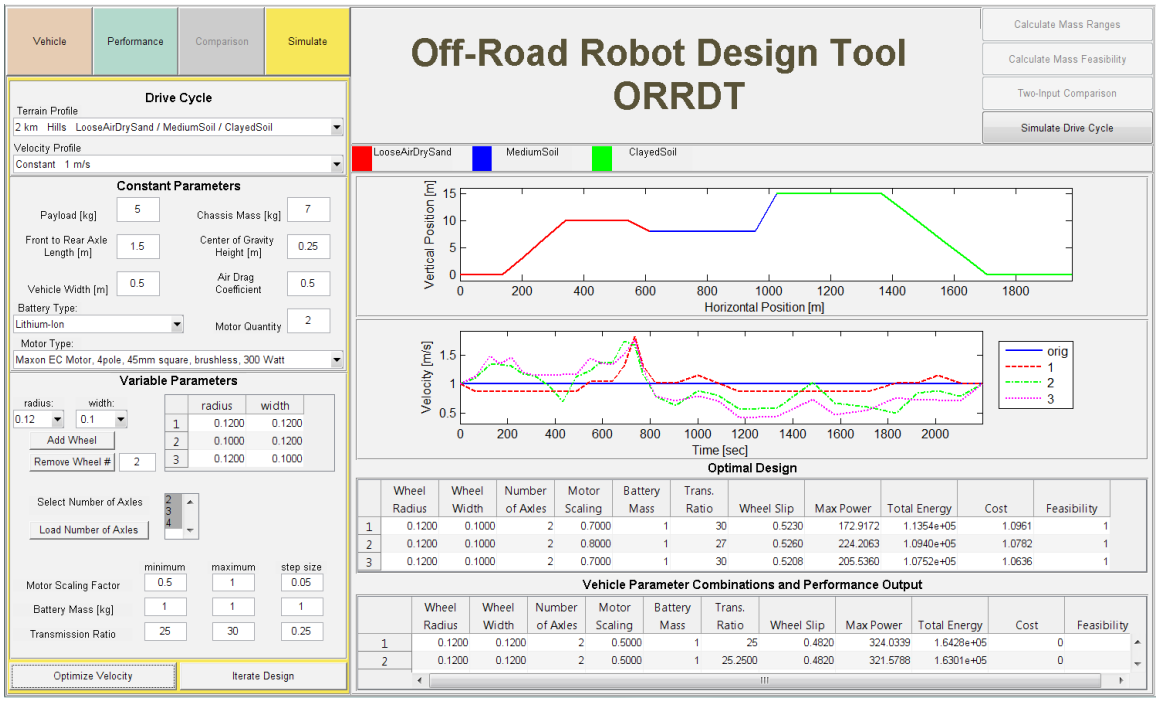

Figure 11. Simulate Panel with Design and Control Optimization Results

Given the relatively short distance of the selected drive cycle, it is not surprising the optimal design has a very small battery. The user must keep in mind practical limitations when specifying limits on parameters such as transmission ratio. The optimal velocity profile shows the vehicle should operate at higher speeds on the dry sand, compared to the medium and clay soil types.

CONCLUSIONS

Vehicle design is a complex process, with interdependencies of a multitude of vehicle parameters. Off-road operation only further complicates the design process, requiring complex wheel-soil interaction modeling. This paper described the development of a design tool, ORRDT, which helps users in the early stages of the design process. Use of wheel tables, developed off-line using terramechanics equations, allowed ORRDT to quickly provide feasibility and efficiency information over a wide range of design and operation parameters. The usefulness of ORRDT was exhibited through a case study.

FUTURE WORK

ORRDT can be expanded to improve its usefulness. Exploration of multiple power source drivetrains could allow for significant improvements in fuel economy and range without losses in performance. Inclusion of tracks, along with wheels, would allow for examination of the tradeoffs in mobility and efficiency. All calculations performed by ORRDT were under the assumption that all values were exact. The user may want not have high confidence in some parameter values, particularly relating to soils. Future versions of ORRDT should account for parameter variability. Finally, ORRDT relies primarily on the current state of wheel-soil interaction modeling using terramechanics. This method requires additional research, especially for small vehicles, to improve calculation accuracy.

DISCLAIMER

NOTATION

ρ density of air = 1.202 (kg/m^3)

CD air drag coefficient

ω wheel rotational velocity (radians/sec)

Ψ ground slope (radians)

A_f maximum vehicle cross sectional area (m^2)

θ_f wheel-soil entry angle (radians)

θ_m angular position of the maximum radial stress (radians)

θ_r wheel-soil exit angle (radians)

θ_{eq} equivalent front-region contact angle for points in the rear-region (radians)

s wheel slip

z wheel sinkage (m)

a_u unloading sinkage

b wheel width (m)

r wheel radius (m)

j shear displacement (m)

c soil cohesion (kPa)

ϕ internal friction angle (radians)

n sinkage exponent

k_c cohesive modulus (kN/m^{n+1})

k_ϕ frictional modulus (kN/m^{n+2})

K_r ratio of residual shear stress to maximum shear stress

K shear modulus (m)

a_0 coefficient for θ_m

a_1 coefficient for θ_m

b_0 coefficient for θ_r

b_1 coefficient for θ_r

k_0 parameter characterizing terrain response to repetitive loading (N/m^3)

A_μ parameter characterizing terrain response to repetitive loading (N/m^4)

APPENDIX: SOIL PARAMETER VALUES[14,20]

Table 3. Soil Parameter Values.[*]

Terrain	c [kPa]	ϕ [rad]	n	k_c [kN/m^{n+1}]	k_ϕ [kN/m^{n+2}]	K [m]
loose, air-dried sand	0	0.478	0.91	-0.66	754.13	0.005
medium soil	8.62	0.393	0.8	29.76	2083	0.0254
clayed soil	7.58	0.244	0.6	30.08	499.7	0.0254

	a_0	a_1	b_0	b_1	k_0 [N/m^3]	A_μ [N/m^4]
loose, air-dried sand	0.18	0.32	0	0	-0.66	$503 \cdot 10^6$
medium soil	0.43	0.32	0	0	29.76	$192.4 \cdot 10^6$
clayed soil	0.43	0.32	0	0	30.08	$63.106 \cdot 10^6$

[*] Medium soil and clayed soil front contact angle parameters could not be obtained. Instead, values for compact sand were used.

APPENDIX: EXAMPLE WHEEL LOOKUP TABLES

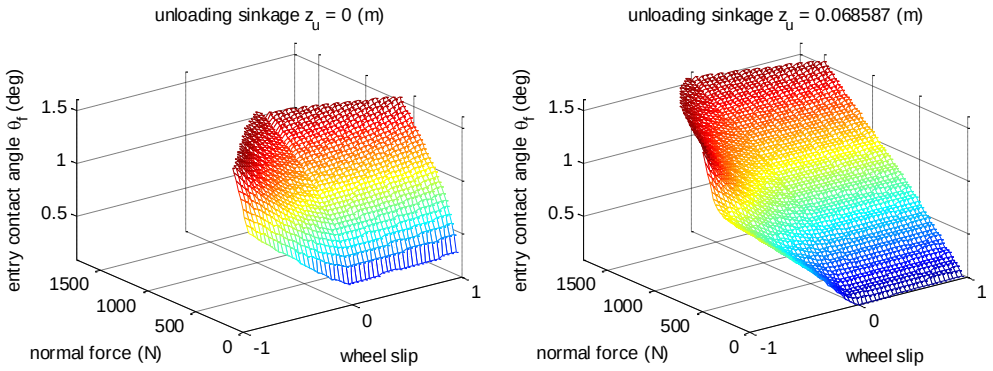

Figure 12. Example Wheel Tables: Entry Contact Angle.

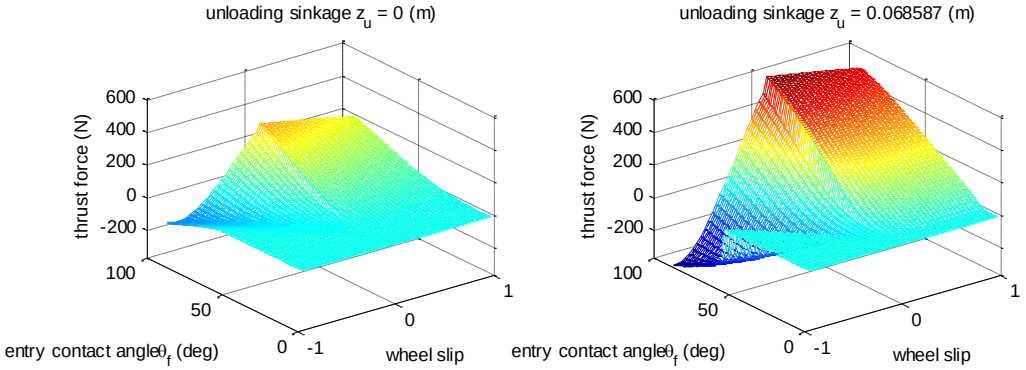

Figure 13. Example Wheel Tables: Thrust Force.

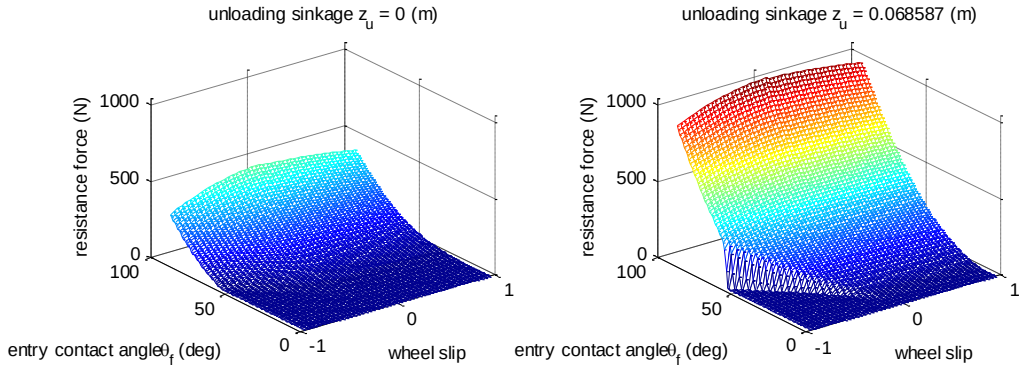

Figure 14. Example Wheel Tables: Resistance Force.

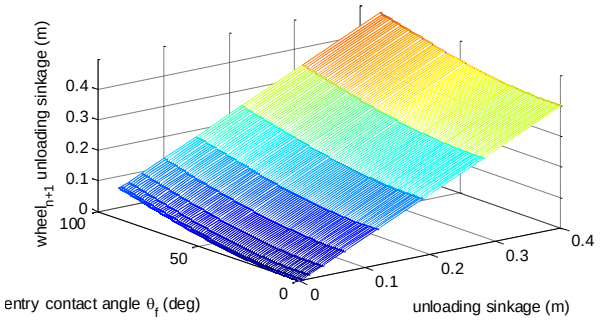

Figure 15. Example Wheel Tables: Unloading Sinkage.

REFERENCES

[1] J. Morales, et al, "Power Consumption Modeling of Skid-Steer Tracked Mobile Robots on Rigid Terrain", *IEEE Transactions on Robotics*. Vol. 25, No. 5, 2009, pp. 1098-1108.

[2] M. G. Bekker, *Theory of Land Locomotion*. The University of Michigan Press. Ann Arbor, MI, 1956.

[3] M. G. Bekker, *Introduction to Terrain-Vehicle Systems*. The University of Michigan Press. Ann Arbor, MI, 1969.

[4] J. Y. Wong, *Terramechanics and Off-road Vehicles*. Elsevier. Amsterdam, 1989.

[5] J. Y. Wong. *Theory of Ground Vehicles, 4th edition*. John Wiley & Sons. Aug, 2008.

[6] K. Iagnemma, S. Kang, H. Shibly, and S. Dubowsky, "Online Terrain Parameter Estimation for Wheeled Mobile Robots with Application to Planetary Rovers." *IEEE Transactions on Robotics*. Vol. 20, No. 5, 2004.

[7] L. Ojeda, J. Borenstein, G. Witus, and R. Karlsen, "Terrain Characterization and Classification with a Mobile Robot." *Journal of Field Robotics*. Vol. 23, No. 2, 2006, pp. 103-122.

[8] G. Meirion-Griffith and M. Spenko, "An Empirical Study of the Terramechanics of Small Unmanned Ground Vehicles." *IEEE Aerospace Conference*, 2010, pp. 1 – 6.

[9] R. Bauer, W. Leung, and T. Barfoot, "Development of a Dynamic Simulation Tool for the Exomars Rover." *Proc. of the 8th International Symposium on Artificial Intelligence, Robotics and Automation in Space – iSAIRAS*. 2005.

[10] P. Poulakis, L. Joudrier, S. Wailliez, and K. Kapellos, "3DROV: A Planetary Rover System Design, Simulation and Verification Tool." *Proceedings 9th International Symposium on Artificial Intelligence, Robotics and Automation in Space (i-SAIRAS)*. 2008.

[11] L. Ding, et al, "Terramechanics-Based High-Fidelity Dynamics Simulation for Wheeled Mobile Robot on Deformable Rough Terrain." *IEEE International Conference on Robotics and Automation*. 2010.

[12] N. Patel, et al, "Rover Mobility Performance Evaluation Tool (RMPET): a Systematic Tool for Rover Chassis Evaluation via Application of Bekker Theory." *Proceedings of the 8th ESA Workshop on Advanced Space Technologies for Robotics and Automation 'ASTRA 2004' ESTEC*. 2004.

[13] C. Nho, J. R. Salton, and B. Spletzer, "Mobility Analysis Tool Based on the Fundamental Principle of Conservation of Energy." *Sandia National Laboratories*. SANDIA Report SAND2007-2791. 2007.

[14] J.Y. Wong. *Terramechanics and Off-Road Vehicle Engineering. Terrain Behaviour, Off-Road Vehicle Performance and Design, Second Edition*. Elsevier, 2010.

[15] Z. Jia, W. Smith, and H. Peng, "Fast Computation of Wheel-Soil Interactions for Safe and Efficient Operation of Mobile Robots." *IEEE/RSJ International Conference on Intelligent Robots and Systems*. 2011.

[16] J.Y. Wong and A.R. Reece, "Prediction of Rigid Wheel Performance Based on the Analysis of Soil-Wheel Stresses - Part II. Performance of Towed Rigid Wheels." *Journal of Terramechanics*, Vol. 4, No. 2, 1967, pp. 7-25.

[17] L. Li and C. Sandu, "On the Impact of Cargo Weight, Vehicle Parameters, and Terrain Characteristics on the Prediction of Traction for Off-Road Vehicles." *Journal of Terramechanics*, Vol. 44, 2007, pp. 221 – 238.

[18] H. Shibly, K. Iagnemma, S. Dubowsky, "An Equivalent Soil Mechanics Formulation for Rigid Wheels in Deformable Terrain, with Application to Planetary Exploration Rovers." *Journal of Terramechanics*, Vol. 42, 2005, pp. 1-13.

[19] C.E. Thomas, "Fuel Cell and Battery Electric Vehicles Compared." *International Journal of Hydrogen Energy, Vol. 34*, 2009, pp. 6005-6020.

[20] J.Y. Wong and A.R. Reece, "Prediction of Rigid Wheel Performance Based on the Analysis of Soil-Wheel Stresses - Part I. Performance of Towed Rigid Wheels." *Journal of Terramechanics*, Vol. 4, No. 1, 1967, pp. 81-98.